# Prognostic value of cardiac inflammation in ST-segment elevation myocardial infarction: A $^{18}$F-fluorodeoxyglucose PET/CT study

Xiao-Ying Xi, MD,[a] Ze Liu, MD,[b] Le-Feng Wang, MD,[c] and Min-Fu Yang, MD[a]

[a] Department of Nuclear Medicine, Beijing Chaoyang Hospital, Capital Medical University, Beijing, China
[b] Department of Cardiology, Peking University Third Hospital Yanqing Hospital, Beijing, China
[c] Center of Cardiology, Beijing Chaoyang Hospital, Capital Medical University, Beijing, China

Received Aug 1, 2021; accepted Oct 24, 2021
doi:10.1007/s12350-021-02858-6

***Background.*** **$^{18}$F-fluorodeoxyglucose (FDG) imaging is used to detect cardiac inflammation and predict functional outcome in acute myocardial infarction (MI). However, data on the correlation of post-MI acute cardiac inflammation evaluated by $^{18}$F-FDG imaging and major adverse cardiac events (MACE) are limited. Therefore, we sought to explore the prognostic value of cardiac $^{18}$F-FDG imaging in patients with acute ST-segment elevation MI (STEMI).**

***Methods.*** **Thirty-six patients with STEMI underwent $^{18}$F-FDG positron emission tomography/computed tomography (PET/CT) 5 days after primary percutaneous coronary intervention. $^{18}$F-FDG activity in infarcted and remote regions, as well as peri-coronary adipose tissue (PCAT), were measured and expressed as the maximum standardized uptake value ($SUV_{max}$). Patients were followed to determine the occurrence of MACE.**

***Results.*** **The infarcted myocardium had a higher $^{18}$F-FDG intensity than the remote area. Moreover, the PCAT of culprit coronary arteries showed a higher $^{18}$F-FDG uptake than that of non-culprit arteries. Multivariate Cox regression analysis showed that increased $SUV_{max}$ of PCAT [HR 5.198; 95% CI (1.058, 25.537), $P$ = .042] was independently associated with a higher risk of MACE.**

***Conclusions.*** **Enhanced PCAT activity after acute MI is related to the occurrence of MACE, and $^{18}$F-FDG PET/CT plays a promising role in providing prognostic information in patients with STEMI. (J Nucl Cardiol 2022;29:3018–27.)**

**Key Words: Myocardial infarction • cardiac inflammation • PCAT • $^{18}$F-FDG • MACE**

Xiao-Ying Xi and Ze Liu have contributed equally to this work and are co-first authors.

**Supplementary Information** The online version contains supplementary material available at https://doi.org/10.1007/s12350-021-02858-6.

The authors of this article have provided a PowerPoint file, available for download at SpringerLink, which summarizes the contents of the paper and is free for re-use at meetings and presentations. Search for the article DOI on SpringerLink.com.

The authors have also provided an audio summary of the article, which is available to download as ESM, or to listen to via the JNC/ASNC Podcast.

**Funding** This study was supported by Beijing Hospitals Authority Clinical Medicine Development of Special Funding Support (ZYLX202105)

Reprint requests: Le-Feng Wang, MD, Center of Cardiology, Beijing Chaoyang Hospital, Capital Medical University, Beijing 100020, China; *wlf311@126.com*, Min-Fu Yang, MD, Department of Nuclear Medicine, Beijing Chaoyang Hospital, Capital Medical University, Beijing 100020, China; *minfuyang@126.com*

J Nucl Cardiol 2022;29:3018–27.
1071-3581/$34.00

| Abbreviations | |
|---|---|
| MI | Myocardial infarction |
| FDG | Fluorodeoxyglucose |
| PET/CT | Positron emission tomography/computerized tomography |
| MACE | Major adverse cardiac events |
| PCAT | Peri-coronary adipose tissue |
| PCI | Percutaneous coronary intervention |
| SUV | Standardized uptake value |
| RCA | Right coronary artery |
| LCX | Left circumflex artery |
| LAD | Left anterior descending artery |

## INTRODUCTION

Acute myocardial infarction (MI) is the leading cause of mortality worldwide. With the improvement of revascularization technology, the survival time post-MI has been prolonged.[1] Nevertheless, the occurrence of long-term adverse cardiac events, such as heart failure and recurrent infarction, has gradually increased over time.[2]

Acute MI can trigger the activation and infiltration of immune cells in the infarcted myocardium.[3] Clinical and experimental studies have suggested that inflammation of the infarcted myocardium plays a key role in the recovery of cardiac function.[4-7] Moreover, a retrospective study revealed that inflammation of the infarcted zone had a tendency to correlate with the clinical prognosis.[8] Intriguingly, the non-infarcted myocardium also showed an increased inflammatory response to acute MI, and the levels of adhesion molecules, chemokines, and matrix metalloproteinase activity were significantly increased in the remote area.[9,10] However, the association of the above changes in the remote myocardium with the clinical outcome has not been fully elucidated.

Peri-coronary adipose tissue (PCAT) inflammation has been reported to drive the formation and progression of atherosclerotic plaque, which is associated with adverse heart events.[11] Previous studies generally assessed PCAT inflammation by measuring the regional fat attenuation on computed tomography (CT) angiography. These studies have suggested that a high PCAT attenuation, linked to increased inflammation, predicts poor prognosis in patients with coronary artery disease.[12,13] In addition, $^{18}$F-fluorodeoxyglucose (FDG) positron emission tomography (PET)/CT has been used to evaluate the PCAT inflammation in the context of coronary atherosclerosis or atrial fibrillation.[11,14] However, the relationship between post-MI PCAT inflammation based on $^{18}$F-FDG PET imaging and prognosis has not yet been investigated.

In summary, the infarcted and remote myocardium and PCAT undergo specific pathological changes following acute MI, and $^{18}$F-FDG imaging can simultaneously assess the inflammatory intensity in these regions. Thus, in this study, we explored the prognostic value of cardiac inflammation imaging with $^{18}$F-FDG in patients with acute MI.

## METHODS

### Study Patients

Between January and December 2016, 467 patients with acute MI underwent primary percutaneous coronary intervention (PCI) in Beijing Chaoyang Hospital. Acute MI was determined according to the third universal definition.[15] Of these patients, 36 patients were recruited to this study according to the following inclusion criteria: (1) ST-segment elevation MI (STEMI); (2) had a single infarct-related coronary artery and no luminal stenosis $>$ 70% in the other coronaries; (3) no prior MI; (4) no history of coronary revascularization (PCI or coronary artery bypass graft); (5) no cardiomyopathy or severe valvular heart disease; (6) no concurrent infectious or other inflammatory diseases; (7) no history of neoplastic disease; and (8) provided consent to participate in the study (Figure 1).

The study was reviewed and approved by the Institutional Ethics Committee of Beijing Chaoyang Hospital (2016-ke-101), and was conducted in accordance with the Declaration of Helsinki. Written informed consent was obtained from all patients.

### Percutaneous Coronary Intervention

Patients received unfractionated heparin to ensure adequate anticoagulation during the invasive procedure. Both coronary angiography and PCI were performed using standard techniques, via either the femoral or radial approach. The stents were placed in the culprit coronary artery. The non-infarct coronary arteries with stenosis $<$ 70% were free of intervention. The decision to use thrombus aspiration and a glycoprotein IIb/IIc inhibitor was at the discretion of the operator. Patients were prescribed dual antiplatelet agents, with statin, beta-blockers, angiotensin-converting enzyme (ACE) inhibitors, or angiotensin receptor blockers (ARB) given as preventive therapy for patients without contraindications.

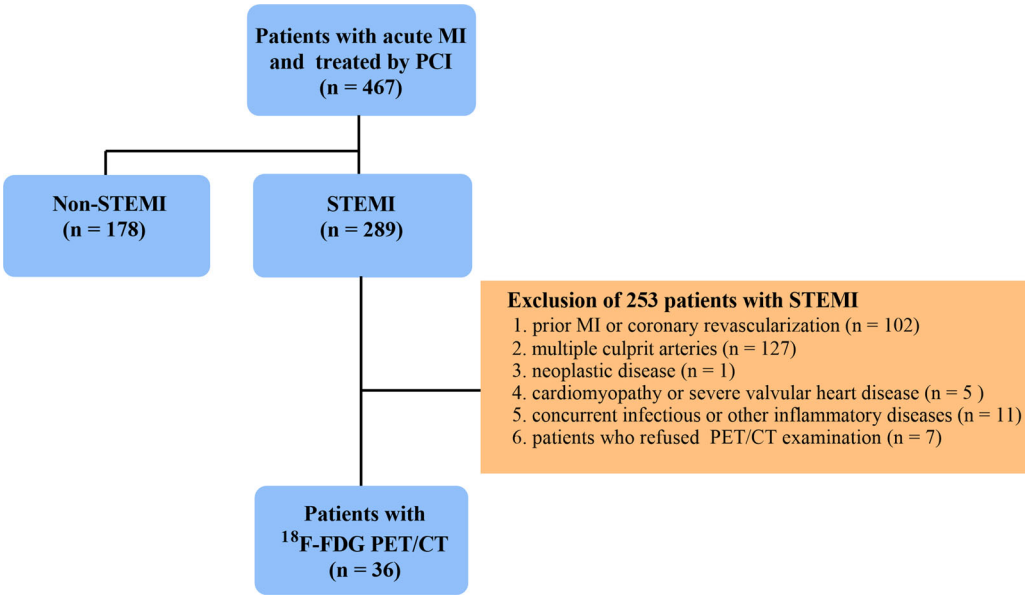


**Figure 1.** Flowchart of patient recruitment.

## Blood Markers

Serial blood markers of myocardial damage and inflammation were obtained following the acute event. Peak levels of creatine kinase (CK), creatine kinase-MB (CK-MB), and troponin I (cTnI), as well as peak white blood cell (WBC), monocyte counts, and hypersensitive C-reactive protein (hsCRP) were taken from this sampling period.

## Cardiac Function

Electrocardiography-gated single photon emission computed tomography (SPECT) myocardial perfusion imaging (MPI) was performed at rest 4.8 ± 1.4 days after PCI for evaluation of cardiac function. Tomographic acquisition was performed 60 minutes after intravenous injection of $^{99m}$Tc-sestamibi (925 MBq) using a dual-detector 90° scanner (Infinia Hawkeye 4, GE, USA) equipped with a low-energy, high-resolution parallel hole collimator centering on the 140 keV photopeak with a 20% symmetric energy window. Sixty images covering 180° (25 seconds per view) were acquired with a matrix of 64 × 64 and a zoom factor of 1.30. The cardiac cycle was divided into 16 equal intervals. Images were reconstructed using a three-dimensional ordered-subset expectation maximization (3D-OSEM) algorithm (10 subsets, 2 iterations), with attenuation and scatter correction. The gated SPECT data were processed and analyzed using an automated program (QGS: version 3.1, Cedars-Sinai Medical Center, Los Angeles, CA, USA). Left ventricular end-diastolic volume (EDV), end-systolic volume (ESV), and ejection fraction (EF) were quantitatively measured.

## $^{18}$F-FDG Imaging and Interpretation

All eligible patients underwent $^{18}$F-FDG imaging 5 days (range 2-9 days) after PCI. To suppress myocardial physiological uptake of $^{18}$F-FDG, all patients received a high-fat, low-carbohydrate diet the evening before imaging, fasted for at least 12 hours before imaging, and were intravenously administered with 50 IU/kg unfractionated heparin 15 minutes before $^{18}$F-FDG injection (360 ± 44 MBq). $^{18}$F-FDG PET/CT imaging was performed 60 minutes after $^{18}$F-FDG administration using a PET/CT scanner (Discovery STE, GE, USA). After scout CT acquisition (120 kV, 10 mA) was used for heart positioning, CT transmission scanning (140 kV, 120 mA) was performed for attenuation correction and anatomical localization. Cardiac PET scan was acquired immediately after CT scanning, with a matrix of 128 × 128, a zoom factor of 2.0, and a photopeak of 511 keV. The scanning time was set to 10 minutes, with one bed position. Images were reconstituted using a 3D-OSEM algorithm (14 subsets, 2 iterations) and were displayed as short-axis, vertical, and horizontal long-axis slices.

Image interpretation was independently performed by two experienced nuclear medicine physicians (XYX and MFY), and disagreements were resolved by consensus. Both observers were blinded to all other clinical information when analyzing images, but were aware of

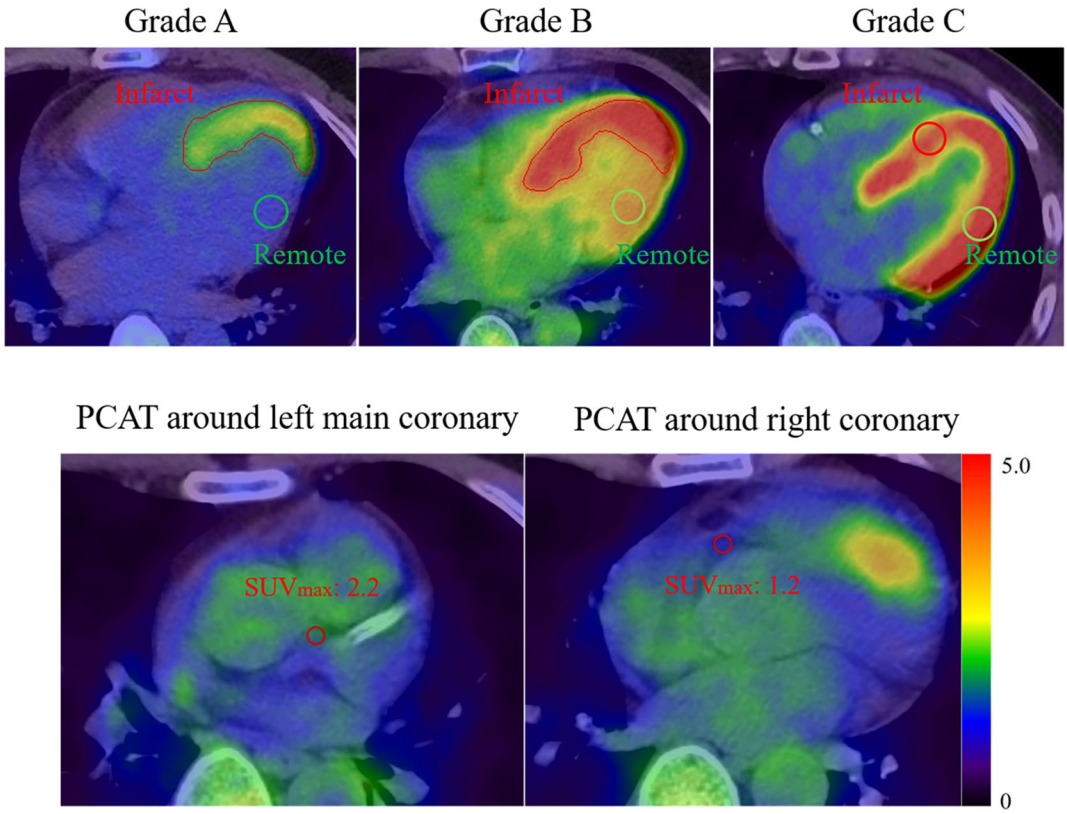


**Figure 2.** Location and semi-quantitative measurement of the infarcted and remote myocardium (upper panel) and peri-coronary adipose tissue (PCAT) (lower panel) on $^{18}$F-FDG PET/CT. Myocardial $^{18}$F-FDG uptake in the remote region was visually graded. Grade A, lower than or equal to blood-pool activity; grade B, higher than the blood-pool but lower than the infarcted area; and grade C, higher than or equal to the infarcted area.

the culprit lesion by looking at the stent on the CT co-registered with PET. First, myocardial $^{18}$F-FDG uptake in the remote (non-culprit coronary dominant) region was visually graded as follows: grade A, lower than or equal to blood-pool activity; grade B, higher than the blood-pool but lower than the infarcted area; and grade C, higher than or equal to the infarcted area (Figure 2). Second, myocardial uptake was quantitatively analyzed using the commercial software package MedEx (MedEx Technology Co. Ltd., Beijing, China). In patients with grade A or B activity in the remote region, the $^{18}$F-FDG uptake volume of the infarcted area was determined by a region grow algorithm with a threshold of 50% of the maximum uptake.[16] The maximum standardized uptake value ($SUV_{max}$) of the infarcted region was also obtained. In patients with grade C activity in the remote area, only the $SUV_{max}$ of the infarcted area was manually measured, and the volume of the infarcted area could not be delineated. The $SUV_{max}$ of the remote area was obtained by manually drawing a circle of 10 mm in diameter in the myocardium opposing the infarct zone oriented by the PET/CT fusion image (Figure 2).

For PCAT measurement, adipose tissue was identified using threshold attenuation values of − 190 to − 30 Hounsfield units. Then, a circle of 5 mm in diameter was drawn on the PCAT adjacent to the left main coronary and proximal right coronary artery (RCA) in the axial PET/CT fusion image, and the $SUV_{max}$ was measured (Figure 2). The former was selected to represent the PCAT activity of the left anterior descending (LAD) and left circumflex (LCX) coronaries, and the latter represented the PCAT activity of the RCA. The circle was manually placed 1 mm away from the coronary outer wall and more than 10 mm away from aortic wall to prevent partial volume effects. Neither myocardial tissue nor the coronary vessel was included in the region of interest. In terms of the manual measurement, $SUV_{max}$ of the region of interest was obtained separately in three continuous slices in the axial PET/CT fusion image and then averaged. Mean of

the measurements taken by two investigators was calculated for further analysis.

### Follow-up

Patients were regularly followed by standardized telephone interviews and by reviewing the medical records. The date of the last follow-up was set to June 1, 2020. The primary endpoint was major adverse cardiac events (MACE), which included all-cause death, hospitalization for nonfatal MI, unstable angina, and late coronary revascularization.

### Statistical Analysis

SPSS version 26.0 (SPSS, Chicago, IL, USA) was used for all statistical analyses. Quantitative data are expressed as mean ± standard deviation or median with an interquartile range based on the distribution of data. The independent-sample t-test or Mann–Whitney *U* test was used for comparison of quantitative variables, as appropriate. Pairwise comparisons were performed using the Wilcoxon signed-rank test. Categorical variables were expressed as number with percentage, and comparisons were performed using Fisher's exact test.

Univariate and multivariable survival analyses were performed using the Cox proportional hazards regression model with the enter method. To make the hazard ratio (HR) comparable, the continuous predictor variables were dichotomized except for the time from MI onset to revascularization. PET-related values and age were dichotomized according to the best cut-offs provided by the receiver operating characteristic analysis, and other variables were based on clinical cut-points. Variables with a $P$-value $< .05$ from the univariate Cox regression were entered into multivariate analysis. The MACE-free survival is displayed using Kaplan–Meier survival curves, and compared using the log-rank test. A $P$-value $< .05$ was considered statistically significant.

## RESULTS

### Patient Characteristics

Among the 36 included patients, 31 (86.1%) were men, with an age of 54.5 ± 10.4 years (range 30.0-69.0 years). The median interval between MI onset and revascularization was 3.2 hours (range 1.3-15.8 h). Intraoperative coronary angiography showed that the culprit artery was the LAD in 22 patients, the RCA in 13 patients, and the LCX in 1 patient. The median level of CK, CK-MB, and cTnI were 1834 U/L, 145 ng/mL, and 56.2 ng/mL, respectively. During hospitalization, all patients were taking aspirin, and more than half of them received statins, Beta-blockers, or ACE inhibitors/ARB (Table 1).

### $^{18}$F-FDG PET/CT

By visual evaluation, most patients (31/36, 86.1%) had higher $^{18}$F-FDG uptake in the infarcted myocardium than in the remote myocardium (grade A: 26 cases; grade B: 5 cases). The $SUV_{max}$ was significantly higher in the infarcted than in the remote myocardium [4.3 (3.6-5.3) vs 1.9 (1.3-2.6), $P < .001$] (Figure 3). PCAT activity in the culprit coronaries was higher than that in non-culprit coronaries [1.4 (1.3-1.7) vs 1.2 (1.1-1.3); $P < .001$; Figure 3].

### Follow-up

Patients were followed for 47 months (range 5-54 months). MACE occurred in nine patients (unstable angina in 6, recurrence of acute MI in 1, cardiac death in 1, late PCI in 1). In the univariate Cox regression analysis, increased $SUV_{max}$ of RCA PCAT [HR 6.273, 95% CI (1.297, 30.343), $P = .022$] and age $> 60$ [HR 6.268, 95% CI (1.296, 30.314), $P = .022$] showed a correlation with a higher risk of MACE. In multivariable Cox regression analysis, they remained significant [increased $SUV_{max}$ of RCA PCAT: HR 5.198, 95% CI (1.058, 25.537), $P = .042$; age $> 60$: HR 5.195, 95% CI (1.057, 25.531), $P = .043$]. The results of univariate and multivariate Cox regression analysis are shown in Table 2 and Figure 4.

## DISCUSSION

In this prospective study, we explored the characteristics of post-MI inflammation in the myocardium and PCAT and its association with MACE. Our results showed that (1) PCAT of the culprit coronary artery had a higher inflammatory activity than that of non-culprit coronary; (2) increased inflammation in PCAT surrounding the RCA predicted a higher risk of MACE; (3) neither the infarcted myocardium nor the remote zone was correlated with MACE risk.

### $^{18}$F-FDG PET/CT in PCAT Post-MI

PCAT is not only recognized as a scaffold for vasculature, but an important paracrine organ that secretes various bioactive molecules (such as interleukin-1β, interleukin-6, and tumor necrosis factor-α).[17-20] These molecules can induce monocytes into the coronary intima-media, which is associated with the extent of plaque progression and stenosis. Moreover, myocardial ischemia can increase the generation of oxidative radicals, which will further activate the

**Table 1.** Patient baseline characteristics

| Variables | All patients (*n* = 36) | MACE+ (*n* = 9) | MACE− (*n* = 27) | *P* |
|---|---|---|---|---|
| Gender, male | 31 (86.1%) | 8 (88.9%) | 23 (85.2%) | 1.000 |
| Age, years | 54.5 ± 10.4 | 61.2 ± 5.4 | 52.3 ± 10.7 | .003* |
| BMI (kg/m$^2$) | 25.5 (24.0-29.0) | 26.0 (23.0-29.0) | 25.0 (24.0-29.0) | .783 |
| Culprit artery location | | | | .316 |
| LAD | 22 (61.1%) | 4 (44.4%) | 18 (66.7%) | |
| LCX | 1 (2.7%) | 0 | 1 (3.7%) | |
| RCA | 13 (36.1%) | 5 (55.6%) | 8 (29.6%) | |
| Time from MI onset to reperfusion, hour | 3.2 (2.5-6.3) | 2.7 (2.0-4.5) | 3.4 (2.6-7.8) | .160 |
| Risk factors of coronary artery disease | | | | |
| Smoking | 25 (69.4%) | 7 (77.8%) | 18 (66.7%) | .690 |
| Family history of cardiovascular disease | 15(41.7%) | 3 (33.3%) | 12 (44.4%) | .705 |
| Hypertension | 17 (47.2%) | 4 (44.4%) | 13 (48.1%) | 1.000 |
| Hypercholesterolemia | 17 (47.2%) | 3 (33.3%) | 14 (51.9%) | .451 |
| Diabetes | 7 (19.4%) | 2 (22.2%) | 5 (18.5%) | 1.000 |
| Medication | | | | |
| Aspirin | 36 (100%) | 9 (100%) | 27 (100%) | 1.000 |
| Statin | 30 (83.3%) | 8(88.9%) | 22 (81.5%) | 1.000 |
| Beta-blocker | 23 (63.9%) | 6 (66.7%) | 17 (63.0%) | 1.000 |
| ACE inhibitor or ARB | 20 (55.6%) | 6 (66.7%) | 14 (51.9%) | .700 |
| Laboratory results | | | | |
| WBC, × 10$^9$/L | 11.2 (8.7-13.6) | 12.4 (10.8-14.0) | 11.0 (8.5-13.1) | .112 |
| Monocytes, × 10$^9$/L | 0.4 (0.3-0.6) | 0.5 (0.3-0.6) | 0.4 (0.3-0.5) | .583 |
| CRP, mg/L | 6.6 (3.0-11.4) | 4.1 (3.0-11.0) | 7.3 (3.0-12.0) | .299 |
| CK, U/L | 1834 (769--2666) | 1846 (633-2733) | 1822 (835-2515) | .898 |
| CK-MB, ng/mL | 145 (66-263) | 115 (29-305) | 146 (72-200) | .826 |
| cTnI, ng/mL | 56.2 (20.3-110.3) | 58.1 (28.4-103.2) | 54.3 (20.2-114.3) | .956 |
| Blood glucose, mg/dL# | 103 (96-123) | 112 (97-120) | 101 (95-126) | .956 |
| Cardiac function | | | | |
| EDV, mL | 87.0 (70.0-117.8) | 78.0 (64.5-91.0) | 96.0 (74.0-119.0) | .070 |
| ESV, mL | 46.0 (37.3-71.5) | 41.0 (36.5-52.0) | 56.0 (38.0-80.0) | .171 |
| EF, % | 46.0 (34.5-51.0) | 47.0 (40.8-51.0) | 46.0 (34.0-53.0) | .956 |

*MACE*, major adverse cardiac events; *BMI*, body mass index; *LAD*, left anterior descending artery; *LCX*, left circumflex artery; *RCA*, right coronary artery; *MI*, myocardial infarction; *ACE*, angiotensin-converting enzyme; *ARB*, angiotensin receptor blocker; *WBC*, white blood cell count; *hsCRP*, hypersensitive C-reactive protein; *CK*, creatine kinase; *CK-MB*, creatine kinase-MB; *cTnI*, troponin I; *EDV*, end-diastolic volume; *ESV*, end-systolic volume; *EF*, ejection fraction
*Indicates statistically significant ($P < .05$).
#Blood glucose level was measured just before the $^{18}$F-FDG injection.

surrounding PCAT inflammation.[21,22] This is in agreement with our finding that PCAT around the culprit coronary artery showed higher $^{18}$F-FDG intensity than that surrounding the non-culprit artery. Similarly, Goeller et al. found that CT attenuation of PCAT, which reflected coronary-specific inflammation, was increased around culprit lesions compared to non-culprit lesions in patients with acute coronary syndrome.[23]

As discussed above, the post-MI inflammation was not uniformly distributed in PCAT; however, the PCAT

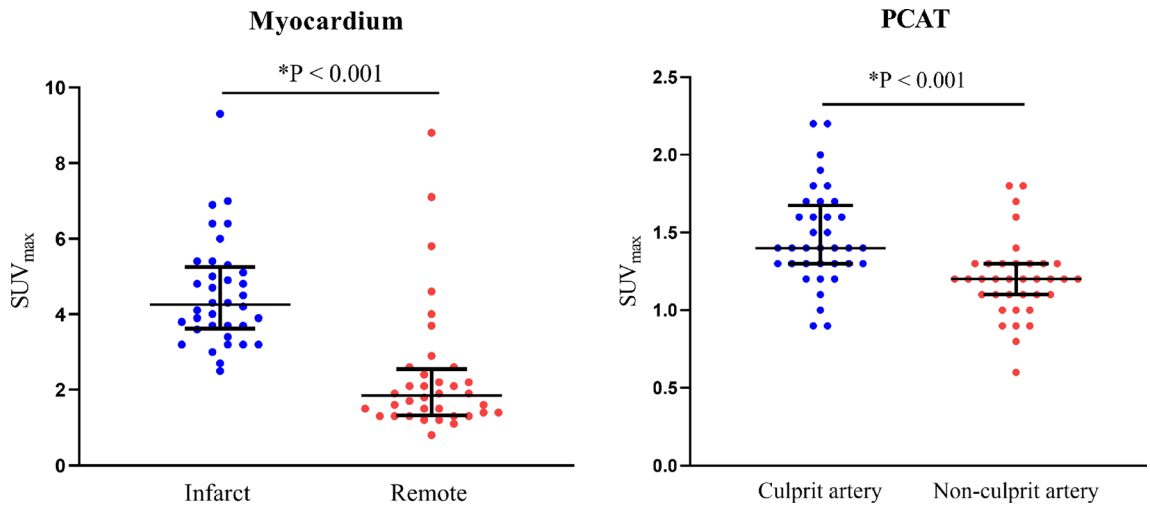


**Figure 3.** $^{18}$F-FDG uptake in the infarcted and remote myocardium and peri-coronary adipose tissue (PCAT). The $^{18}$F-FDG intensity in the infarcted myocardium was significantly higher than that in the remote area. The PCAT of culprit coronary arteries showed a significantly higher $^{18}$F-FDG uptake compared to that of non-culprit arteries.

inflammation in different regions might affect each other due to the lack of physical barriers between different parts of PCAT. A previous study suggested that patients with coronary artery disease had higher global PCAT inflammation than healthy controls.[11] Therefore, it was necessary to select a stable and reproducible region to reflect the real state of global PCAT inflammation. Because the left ventricular myocardium had marked $^{18}$F-FDG uptake following acute MI, the measurement of SUV in PCAT around the LAD or LCX could be interfered by the near left ventricle. In contrast, the PCAT of the RCA was less affected by hindering nonfatty structures and may be a reliable measurement site (inter-observer reliability: .889 for RCA vs .778 for LAD/LCX).

According to previous studies, the PCAT volume or thickness measured by CT or ultrasound can assess or predict the risk of cardiovascular disease.[24-26] In addition, the PCAT density was higher around the inflamed regions such as ruptured plaques or coronary dissections, and can be used to evaluate the inflammation and cardiovascular risk.[23,27-29] To our knowledge, this is the first time that the relationship between post-MI PCAT inflammation and MACE risk has been investigated using $^{18}$F-FDG PET/CT. Herein, the enhanced glucose metabolism in PCAT around the RCA was correlated with the risk of MACE in patients with acute MI.

Van Diemen et al. evaluated the prognostic value of PCAT CT attenuation (PCATa) in 539 patients with suspected coronary artery disease.[12] In line with our findings, they proposed that increased RCA PCATa was associated with a worse prognosis, whereas LAD and LCX PCATa were not correlated with outcome. Moreover, Oikonomou et al. suggested that high perivascular fat attenuation index of the RCA was a suggested surrogate of global coronary inflammation and had a prognostic value in predicting the occurrence of all-cause and cardiac mortality.[13] Because PCAT is more prevalent around the RCA as compared to the LAD/LCX and has less nonfatty tissue in its proximity, the PCAT around RCA may be a more robust and readily accessible measurement of global inflammatory activity and it might explain the superior prognostic value compared to the PCAT of the left coronary system. In addition, the PCAT activity surrounding the culprit artery was not found to correlate with MACE in this study. Nevertheless, we speculated that the inflammatory activity in the PCAT surrounding the culprit artery as well as that in the global PCAT may be higher in patients with acute MI compared to those in healthy populations; thus, both are potential risk factors for coronary inflammation and future MACE.

## $^{18}$F-FDG PET/CT in the Myocardium

In this study, we applied a combined strategy of fasting, low-carbohydrate diet and heparin administration, which has been proven to be effective in suppressing myocardial physiological uptake of $^{18}$F-FDG.[30] Although all patients strictly followed this strategy, five of them (13.9%) still presented with a grade C activity in the remote area. We speculated that the higher $^{18}$F-FDG uptake in the remote area may be related to the regional pathological status, although the

**Table 2.** Univariate and multivariable Cox regression analysis

| | Univariate | | | | Multivariate | | | |
|---|---|---|---|---|---|---|---|---|
| | | 95% CI | | | | 95% CI | | |
| | HR | Lower | Upper | *P* | HR | Lower | Upper | *P* |
| Gender (female as reference) | 1.218 | .152 | 9.741 | .853 | | | | |
| Age > 60 | 6.268 | 1.296 | 30.314 | .022* | 5.195 | 1.057 | 25.531 | .043* |
| BMI > 24 (kg/m$^2$) | 1.134 | .283 | 4.538 | .859 | | | | |
| RCA as culprit artery (LAD + LCX as reference) | 2.495 | .668 | 9.319 | .174 | | | | |
| Time from MI onset to reperfusion, hour | .791 | .560 | 1.116 | .181 | | | | |
| Smoking | 1.679 | .349 | 8.090 | .518 | | | | |
| Family history of cardiovascular disease | .686 | .171 | 2.745 | .594 | | | | |
| Hypertension | .918 | .246 | 3.419 | .898 | | | | |
| Hypercholesterolemia | .505 | .126 | 2.020 | .334 | | | | |
| Diabetes | 1.217 | .253 | 5.867 | .806 | | | | |
| Increased WBC (> 10 × 10$^9$/L) | 1.201 | .937 | 1.540 | .148 | | | | |
| Increased monocytes counts (> .6 × 10$^9$/L) | 1.550 | .322 | 7.466 | .585 | | | | |
| Increased hsCRP (> 3.0 mg/L) | 1.841 | .222 | 15.300 | .572 | | | | |
| Reduced EF (< 50%) | 1.097 | .274 | 4.392 | .896 | | | | |
| $SUV_{max}$ of infarcted myocardium > 4.9# | .477 | .128 | 1.778 | .270 | | | | |
| $SUV_{max}$ of remote myocardium > 2.4# | 2.602 | .698 | 9.704 | .154 | | | | |
| $SUV_{max}$ of RCA PCAT > 1.2# | 6.273 | 1.297 | 30.343 | .022* | 5.198 | 1.058 | 25.537 | .042* |
| $SUV_{max}$ of culprit PCAT > 1.3# | 1.436 | .359 | 5.747 | .609 | | | | |
| $SUV_{max}$ of non-culprit PCAT > 1.1# | 1.436 | .359 | 5.747 | .609 | | | | |

*HR*, hazard ratio; *CI*, confidence interval; *BMI*, body mass index; *LAD*, left anterior descending artery; *LCX*, left circumflex artery; *RCA*, right coronary artery; *MI*, myocardial infarction; *hsCRP*, hypersensitive C-reactive protein; *WBC*, white blood cell count; *EF*, ejection fraction; *PCAT*, peri-coronary adipose tissue; *$SUV_{max}$*, maximum standardized uptake value.
*Indicates statistically significant ($P < .05$).
#PET-related cut-off values were provided by the receiver operating characteristic analysis.

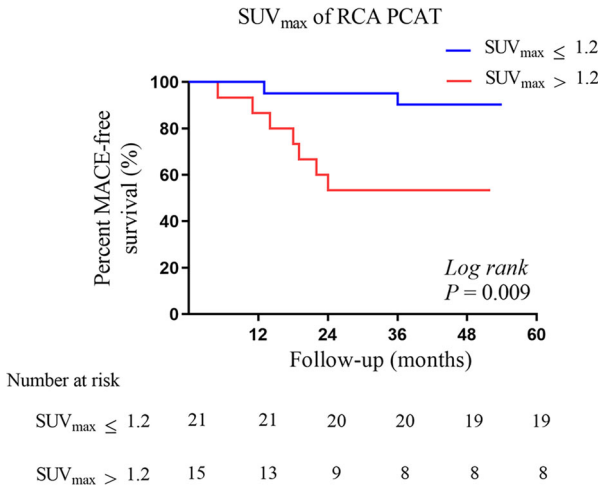


**Figure 4.** Kaplan–Meier curve showing the MACE-free survival rate according to the $SUV_{max}$ of peri-coronary adipose tissue (PCAT) of the right coronary artery (RCA).

underlying mechanism remains unclear. Thus, these five patients were not excluded from the final analysis. Intriguingly, by visual analysis, we found that cases with higher $^{18}$F-FDG uptake in the remote area (grades B and C) had a trend toward a higher incidence of MACE compared to cases with grade A (50.0% vs 15.4%; $P = .079$), although no correlation was found between the $SUV_{max}$ of the remote area and MACE risk according to Cox regression analysis. Similarly, a retrospective study including 15 subjects with acute MI showed that patients who required late coronary revascularization tended to have higher inflammatory activity in the remote zone than those without additional intervention.[8] Further research related to the result is warranted with a larger sample size.

Several studies have investigated the correlation between inflammation in the infarcted area and functional outcome in patients with acute MI.[4-7] However,

few studies have focused on the association between inflammation in the infarcted area and future MACE risk. Wollenweber et al. found that patients with MI without angina symptoms at follow-up showed a trend toward higher inflammatory activity in the infarcted myocardium than those with angina at follow-up.[8] In our study, we found no significant correlation between post-MI $^{18}$F-FDG intensity in the infarcted region and the risk of MACE. Considering that the role of inflammatory responses differed across different post-MI periods,[31] we speculated that the relationship between the inflammation activity in the infarcted area and clinical outcome may not be simply linear.

## Limitations

First, a limited number of patients with acute MI were enrolled in this pilot study. Second, the influence of $^{18}$F-FDG uptake of the left ventricle and coronary artery inflammation on the PCAT SUV measurements could not be excluded due to the partial volume effect. This could lead to an overestimation of PCAT inflammation. Third, although $^{18}$F-FDG imaging was performed median 5 days after PCI, we could not entirely rule out the effect of PCI procedure on the PCAT activity around the culprit artery. The relevant study targeting patients with acute MI and thrombolysis may address this problem. Nevertheless, PCI was performed via standard protocol in all patients and thus might have a similar impact on the global PCAT inflammation. Consequently, this factor was unlikely to confound our result in terms of survival analysis. Forth, although we only included patients with a single culprit coronary artery, non-culprit arteries also had various degrees of stenosis (stenosis degree $< 70\%$) in some subjects. This may complicate the interpretation of the results, but was consistent with the clinical practice.

## NEW KNOWLEDGE GAINED

PCAT inflammation can be assessed using $^{18}$F-FDG PET/CT, and predict the future MACE risks in patients with acute STEMI undergoing PCI.

## CONCLUSIONS

In patients with acute MI undergoing PCI, increased inflammation in PCAT may correlate with a higher risk of MACE. $^{18}$F-FDG PET/CT has the ability to assess inflammatory activity in different regions of the heart and to aid in risk stratification of patients with acute MI.

## Disclosures

*Xiao-Ying Xi, Ze Liu, Le-Feng Wang, and Min-Fu Yang have no conflicts of interest to declare.*

## References

1. Anderson JL, Morrow DA. Acute myocardial infarction. N Engl J Med 2017;376:2053-64.
2. Ezekowitz JA, Kaul P, Bakal JA, Armstrong PW, Welsh RC, McAlister FA. Declining in-hospital mortality and increasing heart failure incidence in elderly patients with first myocardial infarction. J Am Coll Cardiol 2009;53:13-20.
3. Frangogiannis NG. Pathophysiology of myocardial infarction. Compr Physiol. 2015;5:1841-75.
4. Rischpler C, Dirschinger RJ, Nekolla SG, Kossmann H, Nicolosi S, Hanus F. Prospective evaluation of $^{18}$F-fluorodeoxyglucose uptake in postischemic myocardium by simultaneous positron emission tomography/magnetic resonance imaging as a prognostic marker of functional outcome. Circ Cardiovasc Imaging 2016;9:e004316.
5. Ramos IT, Henningsson M, Nezafat M, Lavin B, Lorrio S, Gebhardt P, et al. Simultaneous assessment of cardiac inflammation and extracellular matrix remodeling after myocardial infarction. Circ Cardiovasc Imaging 2018;11:e007453.
6. Dall'Armellina E, Piechnik SK, Ferreira VM, Si QL, Robson MD, Francis JM, et al. Cardiovascular magnetic resonance by non contrast T1-mapping allows assessment of severity of injury in acute myocardial infarction. J Cardiovasc Magn Reson 2012;14:15.
7. Kidambi A, Motwani M, Uddin A, Ripley DP, McDiarmid AK, Swoboda PP, et al. Myocardial extracellular volume estimation by CMR predicts functional recovery following acute MI. JACC Cardiovasc imaging 2017;10:989-99.
8. Wollenweber T, Roentgen P, Schafer A, Schatka I, Zwadlo C, Brunkhorst T, et al. Characterizing the inflammatory tissue response to acute myocardial infarction by clinical multimodality noninvasive imaging. Circ Cardiovasc Imaging 2014;7:811-8.
9. Lee WW, Marinelli B, van der Laan AM, Sena BF, Gorbatov R, Leuschner F, et al. PET/MRI of inflammation in myocardial infarction. J Am Coll Cardiol 2012;59:153-63.
10. Wilk B, Smailovic H, Wisenberg G, Sykes J, Butler J, Kovacs M, et al. Tracking the progress of inflammation with PET/MRI in a canine model of myocardial infarction. J Nucl Cardiol 2021. https://doi.org/10.1007/s12350-020-02487-5.
11. Mazurek T, Kobylecka M, Zielenkiewicz M, Kurek A, Kochman J, Filipiak KJ, et al. PET/CT evaluation of $^{18}$F-FDG uptake in pericoronary adipose tissue in patients with stable coronary artery disease: Independent predictor of atherosclerotic lesions' formation? J Nucl Cardiol 2017;24:1075-84.
12. van Diemen PA, Bom MJ, Driessen RS, Schumacher SP, Everaars H, de Winter RW, et al. Prognostic value of RCA pericoronary adipose tissue CT-attenuation beyond high-risk plaques, plaque volume, and ischemia. JACC Cardiovasc imaging 2021. https://doi.org/10.1016/j.jcmg.2021.02.026.
13. Oikonomou EK, Marwan M, Desai MY, Mancio J, Alashi A, Centeno EH, et al. Non-invasive detection of coronary inflammation using computed tomography and prediction of residual cardiovascular risk (the CRISP CT study): A post-hoc analysis of prospective outcome data. Lancet 2018;392:929-39.
14. Mazurek T, Kiliszek M, Kobylecka M, Skubisz-Gluchowska J, Kochman J, Filipiak K, et al. Relation of proinflammatory activity

of epicardial adipose tissue to the occurrence of atrial fibrillation. Am J Cardiol 2014;113:1505-8.
15. Thygesen K, Alpert J, Jaffe A, Simoons M, Chaitman B, White H, et al. Third universal definition of myocardial infarction. Circulation 2012;126:2020-35.
16. Xi XY, Zhang F, Wang J, Gao W, Tian Y, Xu H, et al. Functional significance of post-myocardial infarction inflammation evaluated by $^{18}$F-fluorodeoxyglucose imaging in swine model. J Nucl Cardiol 2020;27:519-31.
17. Mazurek T, Zhang L, Zalewski A, Mannion JD, Diehl JT, Arafat H, et al. Human epicardial adipose tissue is a source of inflammatory mediators. Circulation 2003;108:2460-6.
18. Cherian S, Lopaschuk GD, Carvalho E. Cellular cross-talk between epicardial adipose tissue and myocardium in relation to the pathogenesis of cardiovascular disease. Am J Physiol Endocrinol Metab 2012;303:E937-49.
19. Keegan J, Gatehouse PD, Yang GZ, Firmin DN. Spiral phase velocity mapping of left and right coronary artery blood flow: Correction for through-plane motion using selective fat-only excitation. J Magn Reson Imaging 2004;20:953-60.
20. Iacobellis G, Corradi D, Sharma AM. Epicardial adipose tissue: Anatomic, biomolecular and clinical relationships with the heart. Nat Clin Pract Cardiovasc Med 2005;2:536-43.
21. Berg G, Miksztowicz V, Morales C, Barchuk M. Epicardial adipose tissue in cardiovascular disease. Adv Exp Med Biol 2019;1127:131-43.
22. Dozio E, Vianello E, Briganti S, Fink B, Malavazos AE, Scognamiglio ET, et al. Increased reactive oxygen species production in epicardial adipose tissues from coronary artery disease patients is associated with brown-to-white adipocyte trans-differentiation. Int J Cardiol 2014;174:413-4.
23. Goeller M, Achenbach S, Cadet S, Kwan AC, Commandeur F, Slomka PJ, et al. pericoronary adipose tissue computed tomography attenuation and high-risk plaque characteristics in acute coronary syndrome compared with stable coronary artery disease. JAMA Cardiol 2018;3:858-63.
24. Cabrera-Rego JO, Escobar-Torres RA, Parra-Jiménez JD, Valiente-Mustelier J. Epicardial fat thickness correlates with coronary in-stent restenosis in patients with acute myocardial infarction. Clin Investig Arterioscler 2019;31:49-55.
25. Balcer B, Dykun I, Schlosser T, Forsting M, Rassaf T, Mahabadi AA. Pericoronary fat volume but not attenuation differentiates culprit lesions in patients with myocardial infarction. Atherosclerosis 2018;276:182-8.
26. Tscharre M, Hauser C, Rohla M, Freynhofer MK, Wojta J, Huber K, et al. Epicardial adipose tissue and cardiovascular outcome in patients with acute coronary syndrome undergoing percutaneous coronary intervention. Eur Heart J Acute Cardiovasc Care 2017;6:750-2.
27. Kwiecinski J, Dey D, Cadet S, Lee SE, Otaki Y, Huynh PT, et al. Peri-coronary adipose tissue density is associated with $^{18}$F-sodium fluoride coronary uptake in stable patients with high-risk plaques. JACC Cardiovasc Imaging 2019;12:2000-10.
28. Antonopoulos AS, Sanna F, Sabharwal N, Thomas S, Oikonomou EK, Herdman L, et al. Detecting human coronary inflammation by imaging perivascular fat. Sci Transl Med 2017;9:eaal2658.
29. Hedgire S, Baliyan V, Zucker EJ, Bittner DO, Staziaki PV, Takx RAP, et al. Perivascular epicardial fat stranding at coronary CT angiography: A marker of acute plaque rupture and spontaneous coronary artery dissection. Radiology 2018;287:808-15.
30. Gao W, Gong J-N, Guo X-J, Wu J-Y, Xi X-Y, Ma Z-H, et al. Value of $^{18}$F-fluorodeoxyglucose positron emission tomography/computed tomography in the evaluation of pulmonary artery activity in patients with Takayasu's arteritis. Eur Heart J Cardiovasc Imaging 2021;22:541-50.
31. Westman PC, Lipinski MJ, Luger D, Waksman R, Bonow RO, Wu E, et al. Inflammation as a driver of adverse left ventricular remodeling after acute myocardial infarction. J Am Coll Cardiol 2016;67:2050-60.